



ELSEVIER

Nuclear Instruments and Methods in Physics Research A 409 (1998) 511–516

---

---

**NUCLEAR  
INSTRUMENTS  
& METHODS  
IN PHYSICS  
RESEARCH**  
Section A

---

---

# A dual detector $\beta$ -ray imaging probe with $\gamma$ -ray background suppression for use in intra-operative detection of radiolabeled tumors

E.J. Hoffman\*, M.P. Tornai, C.S. Levin, L.R. MacDonald, C.H. Holdsworth

*Division of Nuclear Medicine and Biophysics, DoE Laboratory of Structural Biology and Molecular Medicine, B2-086CHS,  
UCLA School of Medicine, 10833 Le Conte Ave., Los Angeles, CA 90095-6948, USA*

---

## Abstract

The basic concepts for a dual detector  $\beta^+$  imaging probe incorporating a method of  $\gamma$ -ray background suppression were evaluated. The test devices consisted of a 1.2 cm<sup>2</sup>  $\beta^+$  imaging CaF<sub>2</sub>(Eu) scintillator disk optically coupled to a 1.7 mm thick, area-matched transparent diffuser disk, which in turn was coupled to sets of 2 × 2 or 4 × 4 mm<sup>2</sup> by 10 mm long BGO, GSO or LSO scintillators, which acted as both  $\gamma$ -detectors as well as light guides for the CaF<sub>2</sub>(Eu) scintillation light, which in turn are attached to a fiber optic bundle coupled to a multichannel photomultiplier. Pulse shape discrimination allowed identification of the detector of interaction and coincidence between the two detectors allowed selection of  $\beta^+$ -only events. This type imaging detector system was shown to be capable of producing high-resolution images of  $\beta^+$  distributions while suppressing the events due to the 511 keV annihilation radiation background. GSO was found to be the detector of choice for this application. © 1998 Elsevier Science B.V. All rights reserved.

---

## 1. Introduction

A series of devices referred to as intraoperative imaging probes have been developed to assist surgeons in locating tumor or tumor remnants during surgery.  $\gamma$ -ray sensitive probes [1–4] can be used to find tumors that have been radiolabeled with  $\gamma$ -ray emitters injected in the patient preoperatively, and  $\beta$ -ray sensitive probes [5–9] are designed to locate tumor remnants, that are labeled with  $\beta$ -emitters

and are employed after the bulk of tumor is removed. The  $\beta$ -probes are sensitive to  $\beta$ -emitters on or just below the surface due to the short range of the beta particles. A number of tumor seeking radiopharmaceuticals have  $\gamma$ -rays emitted in coincidence with the betas and in the case of the positron, the annihilation of the positron produces 2–511 keV  $\gamma$ -rays. Although the beta detector is very thin and made from low Z materials to minimize detection of  $\gamma$ -rays, the  $\gamma$ -rays from distal parts of the body can reach the beta detector and produce a significant background. The problem and some basic concepts for suppressing the  $\gamma$ -ray background have been investigated [10]. The methods

---

\*Corresponding author. Tel.: + 1 310 825 8851; fax: + 1 310 825 4517; e-mail: ehoffman@mail.nuc.ucla.edu.

of suppression either created an imaging probe that was too bulky, or produced a system with a very poor sensitivity. In this work an investigation of a method that does not require additional bulk and produces a minimum loss in sensitivity is reported.

## 2. Materials and methods

The basic concept of the  $\beta$ -imaging probe and the modification for  $\gamma$ -ray suppression is illustrated in Fig. 1. In the original system there were no “phoswich” crystals, simply a fiber optic coupling to the MC-PMT, and the signal from each fiber/channel used a resistive divider network to produce a signal that gave an output proportional to its position [6,8]. The signals are fed to ADCs and the centroid position of each event is calculated to give an image of the distribution of activity in the tissue.

The addition of the “phoswich” crystals allows the simultaneous detection of beta and gamma events. When the  $\text{CaF}_2(\text{Eu})$  crystal and the “phoswich” crystal detect an event at the same time, the probability of the event coming from the same nucleus or same positron annihilation is very high for the low counting rates expected in the actual use of the system. When a positron is absorbed in the  $\text{CaF}_2(\text{Eu})$  crystal, it will deposit its kinetic energy in the crystal and then annihilate, producing two back-to-back 511 keV photons. Because of the large solid angle there is more than a 50% probability that one of the photons will be intercepted by one of the phoswich detectors. Similar geometrical arguments can be made for single gammas emitted from the nucleus in coincidence with the betas, since the isotope must be essentially touching the face of the detector to be detected. In the latter case, if only one gamma is emitted, the sensitivity would be reduced by a factor of two (but it will increase with the multiplicity of gammas).

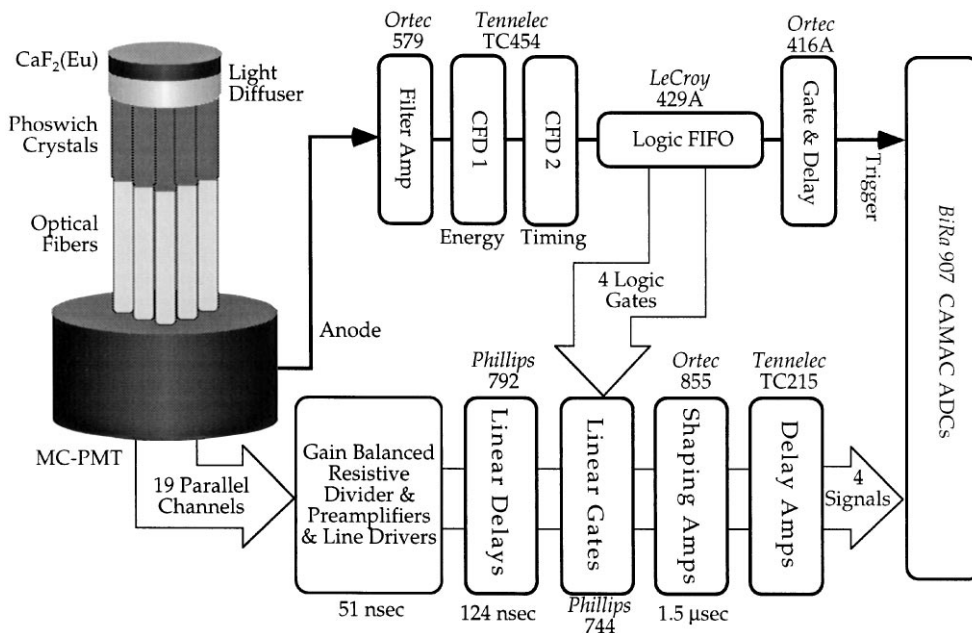


Fig. 1. Diagram of  $\beta$ -imaging probe with  $\gamma$ -background suppression. On left is  $\text{CaF}_2(\text{Eu})$  scintillator disk for  $\beta$ -detection, which is optically connected to diffuser disk, sets of transparent  $\gamma$ -ray scintillation detectors and fiber optics. Scintillation light is detected by a Multichannel Photomultiplier (MC-PMT) and these signals are processed to provide position information in the lower pathway, providing a signal to calculate centroid position of each event. Upper path provides total energy and timing to allow discrimination between betas and gammas.

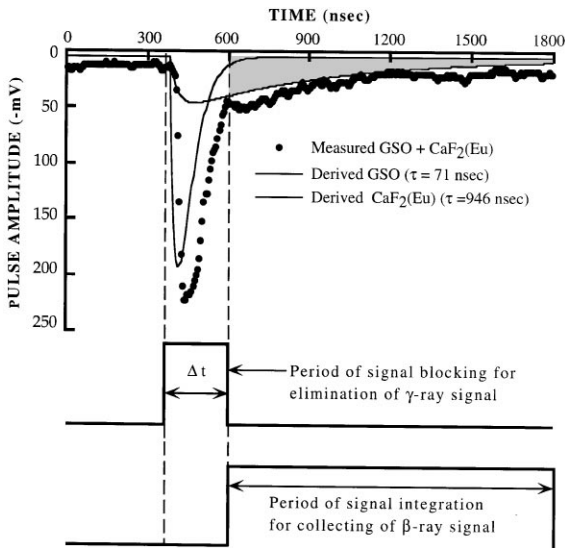


Fig. 2. Measured digital oscilloscope signal for  $\text{CaF}_2(\text{Eu})$  (slow) and GSO (fast) scintillators detecting simultaneous positron and annihilation gamma events. The smooth curves are derived from fits to the data. The position of a logic pulse ( $\Delta t$ ) is indicated and it overlaps a majority of the  $\gamma$  portion of the simultaneous events. This logic pulse blocks the signal from passing through a linear gate. The second logic signal corresponds to the shaded region in the scope trace, and signal integration is allowed in this region.

One difficulty with the system, as described thus far, is the fact that the signal is following a common path at the same time for both crystals for valid events. The beta signal carries the position information, while the gamma signal can be in any channel and carries no useful information, except the fact that it is in coincidence with the beta signal. The key to the operation is the difference in the scintillation decay constants of the various scintillators.  $\text{CaF}_2(\text{Eu})$  has a relatively long decay time of  $\sim 940$  ns, while the phoswich candidates, Bismuth Germanate (BGO), Gadolinium Orthosilicate (GSO), and Lutetium Orthosilicate (LSO) have decay times of about 300, 60, and 40 ns, respectively. In Fig. 2, the average signal from a digital oscilloscope is shown for a number of coincidence events between  $\text{CaF}_2(\text{Eu})$  and GSO.

From Fig. 2, it can be seen that there are two features of the signal that can be used for gamma background suppression. The first is the use of

energy discrimination. If the  $\gamma$  and  $\beta$  energies are absorbed simultaneously in their respective detectors, the amplitude of the sum will exceed the maximum possible for either particle alone. Thus, by setting the threshold on the fast signal above the maximum  $\gamma$  energy, only  $\gamma + \beta$  events are selected. Secondly, if the signal integration is blocked for a period corresponding to  $> 3$  times the decay time of the phoswich scintillator, less than 5% of the  $\gamma$  signal will be available to contaminate the  $\beta$  imaging signal.

Various combinations of energy threshold, signal blocking time, and crystal type and geometry were evaluated. The ideal phoswich crystal geometry would be a one-to-one match with the 2 mm diameter optical fiber. The crystals available were  $2 \times 2 \text{ mm}^2$  by 10 mm long BGO and LSO crystals (19), which were an approximate match to the 19 two millimeters diameter optical fibers, and  $4 \times 4 \text{ mm}^2$  by 10 mm long LSO and GSO crystals (7). Test sources were: (1)  $^{18}\text{F}$  point sources, (2) a source that produces an image of a  $\beta^+$ , which was made by drilling the pattern in plastic as shallow holes, 0.5 mm diameter by  $\sim 1.0$  mm deep, and pipetting about  $4 \mu\text{l}$  of  $^{18}\text{F}$  solution into each hole and covering each hole with a transparent tape (This approximates the environment of tumor remnants near the surface in surgery.) and (3) background was provided by  $^{18}\text{F}$  activity in a 400 ml beaker placed behind source 2.

### 3. Results

The image of a point source of  $^{18}\text{F}$  was taken with each crystal type and geometry as a function of energy threshold and width of the  $\gamma$ -signal blocking window. Fig. 3 shows the result of one such measurement using the  $4 \times 4 \times 10 \text{ mm}^3$  LSO phoswich crystals. The point source coincides with the central element of the seven LSO crystals. The images in the lower left illustrate the problem of the contamination of the  $\beta^+$  image signal by the  $\gamma$ -signals in the phoswich detectors. The  $\gamma$ -signals are clearly an unacceptable background and should be eliminated. This background can be decreased by increasing the blocking window width, increasing the energy threshold or using some combination of

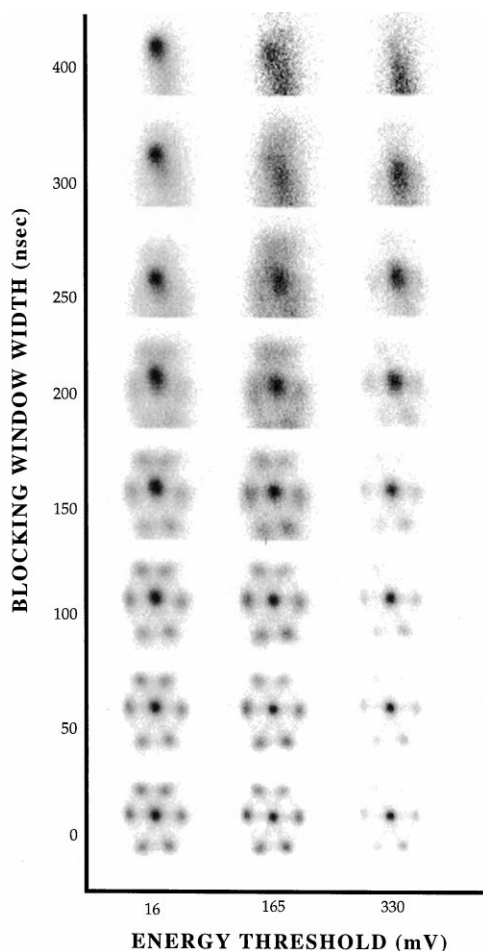


Fig. 3. Image of a  $^{18}\text{F}$  point source as a function of energy threshold and blocking window time. The point source overlaps the central element of the  $4 \times 4$  by  $10 \text{ mm}^3$  7-element phoswich detector.

both. Simply increasing the blocking window width has the problem that this also decreases the fraction of the  $\beta^+$  imaging signal that is integrated and this leads to poorer image resolution because of the poorer precision of the positioning signal. Increasing the energy threshold tends to improve the spatial resolution by selecting only the largest signals for integration. Unfortunately this also eliminates many events and will lower the sensitivity of the system.

Fig. 4 shows a summary of the results of the point source measurement for the various crystals and geometries. These results are for the lowest

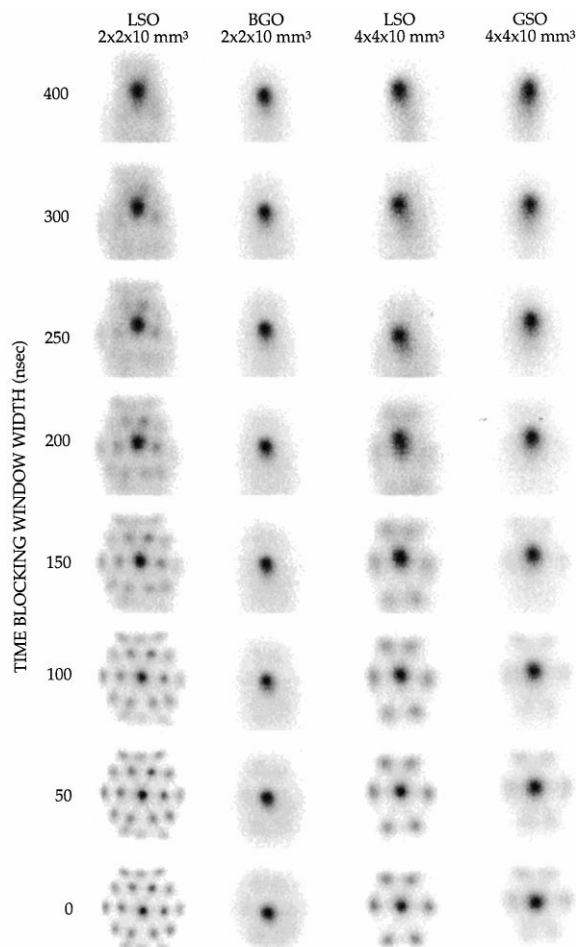


Fig. 4.  $^{18}\text{F}$  point source images for the various phoswich crystals and geometries. The energy threshold is fixed at the lowest possible level and the blocking window width is varied.

energy threshold that is still above noise for the system. As expected the spatial resolution is best for the  $2 \times 2 \text{ mm}^2$  crystals (LSO column). The low light of BGO does not allow the individual phoswich crystals to be resolved. The point source image has poorer spatial resolution for BGO, which may be due to its very high index of refraction (2.2) interfering with the transmission of light to the MC-PMT. The very high light output of the LSO causes its  $\gamma$ -signal to be visible for very wide blocking windows (250 ns +). The GSO  $\gamma$ -signal is suppressed significantly at 100–150 ns.

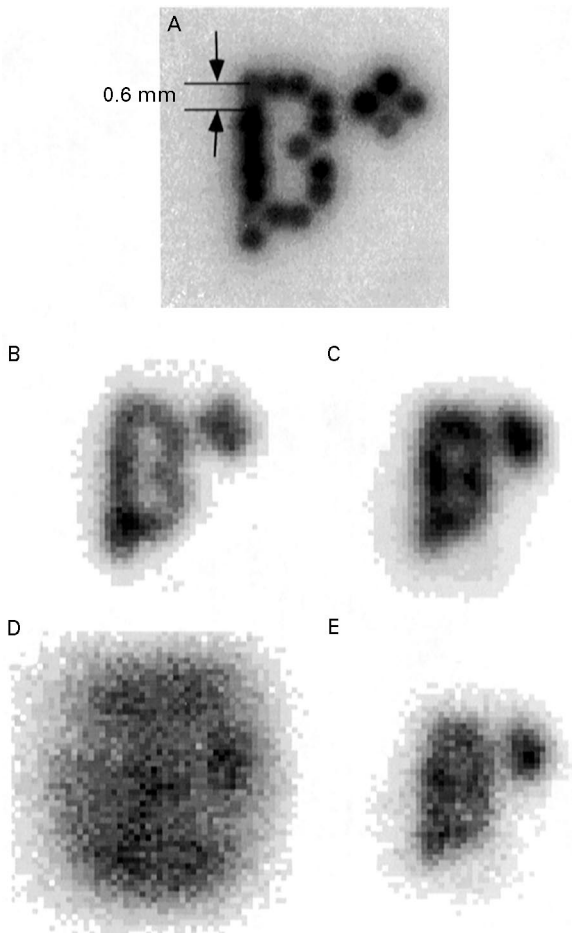


Fig. 5. Images of the  $\beta^+$  test object: (A) Images with an autoradiographic system with  $25\ \mu\text{m}$  FWHM spatial resolution. (B) Images with original  $\beta$  imaging probe (0.6 mm FWHM). (C) Images with phoswich imaging probe (1.3 mm FWHM). (D) Images with 0.25 mCi in background without phoswich background suppression. (E) Image under same conditions as (D), but with phoswich background suppression.

Fig. 5 show a series of images of the  $\beta^+$  test object or phantom. Fig. 5A shows the ideal image, which was obtained with an autoradiographic system that has  $25\ \mu\text{m}$  resolution. The difficulty of exact volume measurements at the  $4\ \mu\text{l}$  level is obvious from the variable intensity of the dots. Fig. 5B shows an image taken with the original  $\beta$  imaging probe which has a resolution of 0.6 mm FWHM, and 5C is taken with BGO phoswich probe ( $2 \times 2\ \text{mm}^2$ ) with 1.3 mm FWHM resolution. Without external background, both systems have

good image contrast. In Fig. 5D, a 0.25 mCi background has been added, and without using the phoswich background suppression almost none of the features of the  $\beta^+$  can be visualized. In Fig. 5E, the phoswich background suppression is used and the contrast approaches that seen in Fig. 5C, removing a very large fraction of the background.

#### 4. Discussion and conclusions

A method of suppressing  $\gamma$ -ray background for an intraoperative imaging probe that is designed to detect  $\beta$ s was described and given a preliminary evaluation. When the beta is a positron, the  $\gamma$ -rays are inherent to the decay process. If there are coincident  $\gamma$ -rays associated with the isotope, the magnitude of the problem is smaller, however, the level of effectiveness of the background suppression is also less with this technique. The crystal geometries available were not ideal, but the results did show effective background suppression and good resolution. Our surgeon collaborators felt that 5 mm FWHM resolution would be adequate for their work. Therefore, we are well within the perceived requirements of the technique with the 1.3 mm resolution that was achieved.

The best overall combination of properties was achieved with GSO. LSO produced too much light which made it difficult to suppress the background. BGO has a decay time that is too long and seems to have problems in light transmission. The next step will be to obtain 2 mm diameter GSO crystals to match the optical fibers to see if we can come close to matching the standard system in spatial resolution.

#### Acknowledgements

This work was funded in part by NIH/NCI Grant R01-CA61037, T32-CA09092, and DOE contract DE-FC03-87-ER60615.

#### References

- [1] B.E. Patt, J.S. Iwanczyk, M.P. Tornai, C.S. Levin, E.J. Hoffman, Nucl. Instr. and Meth. A 366 (1995) 173.

- [2] B.E. Patt, J.S. Iwaczyk, Y.J. Wang, M.P. Tornai, C.S. Levin, E.J. Hoffman, *Nucl. Instr. and Meth. A* 380 (1996) 295.
- [3] M.P. Tornai, C.S. Levin, L.R. MacDonald, E.J. Hoffman, J. Park, *IEEE Trans. Nucl. Sci. NS-44* (1997) in press.
- [4] B.E. Patt, M.P. Tornai, J.S. Iwaczyk, E.J. Hoffman, C.S. Levin, *IEEE Trans. Nucl. Sci. NS-44* (1997) in press.
- [5] L.R. Macdonald, M.P. Tornai, C.S. Levin, J. Park, D.B. Cline, M. Atac, E.J. Hoffman, *IEEE Trans. Nucl. Sci. NS-42* (1995) 1351.
- [6] M.P. Tornai, L.R. Macdonald, C.S. Levin, S. Siegel, E.J. Hoffman, *IEEE Trans. Nucl. Sci. NS-43* (1996).
- [7] C.S. Levin, L.R. Macdonald, M.P. Tornai, E.J. Hoffman, J. Park, *IEEE Trans. Nucl. Sci. NS-43* (1996) 2053.
- [8] M.P. Tornai, E.J. Hoffman, L.R. Macdonald, C.S. Levin, *IEEE Trans. Nucl. Sci. NS-43* (1996).
- [9] L.R. Macdonald, M. Tornai, C.S. Levin, J. Park, M. Atac, D.B. Cline, E.J. Hoffman, *Proc. SPIE* 2551 (1996) 92.
- [10] C.S. Levin, M.P. Tornai, L.R. Macdonald, E.J. Hoffman, *IEEE Trans. Nucl. Sci. NS-44* (1997) in press.